Available online at www.sciencedirect.com
ScienceDirect
Journal of Power Sources 168 (2007) 172–177
JOURNAL OF POWER SOURCES
www.elsevier.com/locate/jpowsour

Short communication

Synthesis and properties of fluorine-containing polybenzimidazole/montmorillonite nanocomposite membranes for direct methanol fuel cell applications

Shih-Wei Chuang, Steve Lien-Chung Hsu *, Chiao-Ling Hsu

Department of Materials Science & Engineering, National Cheng-Kung University, Tainan, Taiwan ROC

Received 12 January 2007; received in revised form 11 March 2007; accepted 12 March 2007
Available online 15 March 2007

Abstract

Novel polybenzimidazole (PBI)/montmorillonite (MMT) nanocomposite membranes were prepared from an organosoluble, fluorine-containing PBI with an organically modified MMT (m-MMT) clay. Both wide angle X-ray diffraction (WAXD) and transmission electron microscopy (TEM) analyses showed that the m-MMT was well dispersed in the PBI matrix on a nanometer scale. The thermooxidative stability of PBI membranes increased slightly with the increase of m-MMT content. The coefficients of the thermal expansion (CTE) of PBI/7 wt% m-MMT nanocomposite membranes were decreased by 30% relative to that of pure PBI. The mechanical properties and the methanol barrier ability of the PBI films were significantly improved by the addition of m-MMT. The tensile modulus of PBI/5 wt% m-MMT nanocomposite membranes had a 41% increase compared to the pure PBI films. The m-MMT in the phosphoric acid-doped PBI could effectively inhibit the plasticizing effect of the phosphoric acid. The methanol permeability of the PBI/5 wt% m-MMT nanocomposite membrane decreased by approximately 81% with respect to the pure PBI membranes. The conductivity of the acid-doped PBI/m-MMT nanocomposites was slightly lower than the acid-doped pure PBI.
© 2007 Elsevier B.V. All rights reserved.

Keywords: Polybenzimidazole; Nanocomposite; Fuel cell; Montmorillonite

1. Introduction

The direct methanol fuel cell (DMFC) has received a lot of attention in recent years, because of its high efficiency and light weight compared to other fuel cell systems. Polymer membranes play an important role as the proton exchange membrane in DMFC. It is well known that the most widely used membranes in DMFC are Nafion®, the perfluorosulfonic acid polymer membranes, owing to their outstanding chemical stability and high proton conductivity. Nevertheless, there are two major drawbacks in Nafion® that must be overcome. First, the proton conductivity of Nafion® is unstable at temperatures above 100 °C, because of dehydration. Second, high methanol permeation through Nafion® membranes not only causes loss of fuel, but also decreases cathode performance in DMFC [1–5]. Recently, polybenzimidazole (PBI) has emerged as a promising candidate for high-temperature (>100 °C) fuel cell applications, because of its high thermal stability and good mechanical properties. In particular, PBI doped with strong acid has stable proton conductivity at temperatures higher than 100 °C, which gives it the potential for use as high-temperature fuel cell proton exchange membrane [6–14].

For the reduction of the methanol permeability through the membranes, several studies showed that the addition of inorganic fillers is able to improve the barrier properties of several polymers (e.g. poly(ether ether ketone), poly(vinyl alcohol), perfluorosulfonic acid, etc.) towards various gases and moisture [15–21]. Montmorillonite (MMT) is a well known layered silicate, which can be used as a nanofiller in polymers, because of its high aspect ratio and low price [22–28]. The layer structure of MMT is expected to be able to decrease the methanol permeation through polymer membranes due to a winding diffusion pathway for methanol.

In this work, we attempted to prepare PBI/MMT nanocomposite membranes for high-temperature fuel cell applications. The most common PBI used in proton exchange membrane

* Corresponding author. Tel.: +886 6 2757575x62904; fax: +886 6 2346290.
E-mail address: lchsu@mail.ncku.edu.tw (S.L.-C. Hsu).

0378-7753/$ – see front matter © 2007 Elsevier B.V. All rights reserved.
doi:10.1016/j.jpowsour.2007.03.021

for fuel cells is based on poly[2,2′-(*m*-phenylene)-5,5′-bibenzimidazole]. However, the PBI is difficult to dissolve in common organic solvents due to its very rigid molecular structure, so it is hard to incorporate MMT into PBI to prepare a nanocomposite. In our previous paper, we have prepared an amorphous, organosoluble fluorine-containing PBI for high-temperature fuel cell applications [29]. The fluorine-containing PBI is expected to have good compatibility with an organically modified MMT (m-MMT), which we have reported before [30]. Here, we report the use of the fluorine-containing PBI to prepare nanocomposite membranes with m-MMT, and discuss the effect of m-MMT on the properties of membranes for DMFC applications.

2. Experimental

2.1. Materials

2,2-Bis(4-carboxyphenyl)hexafluoropropane was purchased from TCI and purified by recrystallization from glacial acetic acid. 3,3′-Diaminobenzidine, dodecylamine (DOA), and dimethylacetamide (DMAc) were obtained from Aldrich. 3,3′-Diaminobenzidine and DOA were used as received, and DMAc was purified by distillation over calcium hydride. Reagent-grade poly(phosphoric acid) (PPA) and phosphoric acid were obtained from Fluka and used as supplied. MMT clay with a cation-exchange capacity of 95 meq 100 g^{-1} was obtained from Pai Kong Co. (Tauyan, Taiwan). Other chemicals and solvents were used as received.

2.2. Polymer synthesis and MMT modification

PBI was synthesized from 3,3′-diaminobenzidine and 2,2-bis(4-carboxyphenyl)hexafluoropropane by the condensation polymerization in PPA at 200 °C, according to Scheme 1. The detailed synthesis procedure was reported in our previous paper [29]. The organically modified MMT (m-MMT) clay was prepared by a cation-exchange reaction between MMT and an ammonium salt of DOA as described in our earlier research [30]. The interlayer spacing of MMT was 12.7 Å. After modification, the interlayer spacing of the m-MMT was expanded to 18 Å.

2.3. Preparation of PBI/MMT nanocomposite membranes

A representative 5 wt% m-MMT loading PBI/m-MMT nanocomposite was prepared as follows: 0.026 g of m-MMT was dispersed in 2 g of DMAc at room temperature under vigorous stirring for 1 h by a mechanical stirrer, and then added to a PBI solution, which was prepared by dissolving 14.64 g of PBI in DMAc to form a 3 wt% solution. The mixture was vigorously stirred for 24 h to make a homogeneous solution. The solution was cast onto a glass plate with a doctor's knife and dried in a vacuum oven at 80 °C for 24 h to remove the solvent. The thickness of the PBI/m-MMT nanocomposite membranes was approximately 40 μm. The membranes were doped by immersion in aqueous phosphoric acid (11 M) for different times. The amount of phosphoric acid in each film was dependent on the immersion time, and calculated by weight analysis. The phosphoric acid-doped PBIs were coded as PBI-$x$$H_3PO_4$, with x as the number of moles of acid per repeat unit of PBI.

2.4. Characterization

The inherent viscosity was measured with a Cannon-Ubbelohde no. 100 viscometer at a concentration of 0.5 g dL^{-1} in DMAc at 30 °C. The wide angle X-ray diffraction (WAXD) experiment was conducted on a Rigaku (Tokyo, Japan) D/MAX-IIIV X-ray diffractometer with Cu Kα radiation. The samples for transmission electron micrograph (TEM) study were prepared by placing the PBI/m-MMT nanocomposite films in an epoxy resin, cured at 70 °C overnight. The cured epoxies containing PBI/m-MMT were microtomed with a diamond knife into 50-nm-thick slices. Next, they were placed on a 200-mesh copper grid and examined with a JOEL JEM-1200EX TEM using an acceleration voltage of 200 KV. The thermoxaditive stability was analyzed with a TA Instrument 2050 Thermogravimetric analyzer (TGA) at a heating rate of 10 °C min^{-1} under air. The in-plane coefficients of thermal expansion (CTEs) and dynamic thermal mechanical analysis (DTMA) of PBI/m-MMT nanocomposite membranes were determined using a TA Instrument Thermal Mechanical Analyzer (TMA) Q400EM. The CTEs were measured with an extension probe under 0.05N tension force on the films in the temperature range of 100–250 °C

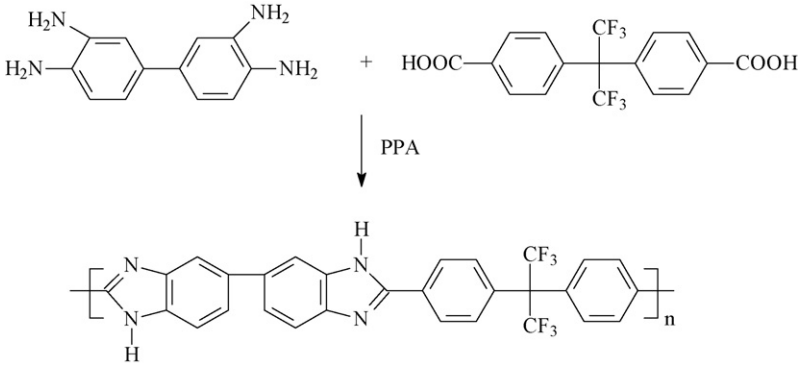

Scheme 1. Synthesis of the fluorine-containing PBI.

at a heating rate of 5 °C min^{-1} under nitrogen. The DTMA was measured at a heating rate of 5 °C min^{-1} in nitrogen under a modulated force of 0.05 N at a frequency of 1 Hz. Tensile properties were determined from stress–strain curves obtained with a Shimadzu AG-SI universal testing machine at a strain rate of 5 mm min^{-1} at room temperature. The film specimens were 30 mm long, 4.5 mm wide, and 40 μm thick. The conductivity measurement was performed with an Autolab PGSTST 30 impedance analyzer in the frequency range of 100–10^5 Hz with amplitude of 10 mV. The measurements were taken at 160 °C under anhydrous condition. The conductivity (σ) was calculated as follows:

$$\sigma = \frac{1}{R}\frac{L}{A}$$

where R, L, and A are the measured resistance, thickness, and cross-sectional area of the membrane, respectively. The methanol permeability was measured with a two-compartment glass cell. One source cell (V_A = 100 mL) was filled with a 6 wt% methanol aqueous solution. The other receiving cell (V_B = 100 mL) was filled with deionized water. The membrane was clamped between the two compartments. The concentration of methanol in the receiving cell was measured versus time by gas chromatography with a Shimadzu QP2010. The methanol concentration in the receiving cell is given by

$$C_B(t) = \frac{A}{V_B}\frac{P}{L}C_A(t - t_o)$$

where C_B and C_A are the methanol concentration in the receiving cell and the source cell, respectively; V_B the volume of the receiving cell; and P the methanol permeability. t_o, also termed the time lag, is related to the methanol diffusion coefficient (D) as follows: $t_o = L^2/6D$ [31,32].

3. Results and discussion

3.1. Preparation of PBI/m-MMT nanocomposite membranes

In order to disperse the hydrophilic MMT to the PBI matrix, the MMT was first treated with the ammonium salt of dodecylamine to form an organoclay through a cation-exchange reaction. The m-MMT is compatible with the organic solvent, DMAc and the PBI polymer, since the 3 and 5 wt% m-MMT loading PBI solutions and the resulting membranes are visually clear. The fluorine-containing PBI is soluble in DMAc, which makes the mixing of the m-MMT to PBI possible through a solution process. The inherent viscosity of the polymer was 1.9 dL g^{-1} measured in DMAc at a concentration of 0.5 g dL^{-1} at 30 °C. Due to the high molecular weight, the PBI and PBI/m-MMT membranes are strong and tough, which can be used for fuel cell applications.

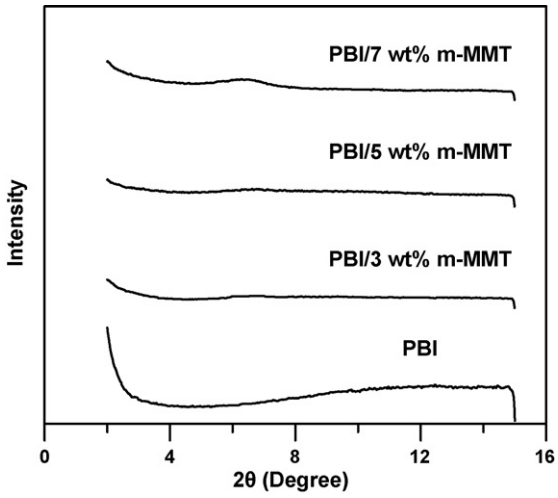

Fig. 1. WAXD patterns of PBI/m-MMT nanocomposite membranes.

3.2. Dispersion of MMT in PBI matrix

The dispersion of organoclay in the polymer matrix can be observed from the WAXD analysis. Fig. 1 shows the WAXD patterns of PBI/3-7 wt% m-MMT nanocomposites. The 3 and 5 wt% m-MMT loaded nanocomposites do not have any diffraction peak in the range 2θ = 2–10°. This indicates an exfoliated dispersion of m-MMT in the PBI matrix. When m-MMT reaches 7 wt% in PBI matrix, a small peak appears at 6.28° (the interlayer spacing = 14.1 Å). The crystalline peak implies that some of the silicate layers have aggregated in the PBI matrix. TEM micrographs of PBI/3–7 wt% m-MMT nanocomposites are shown in Fig. 2. The black lines in the figure are the cross-sections of the m-MMT silicate layers, and the grey part is the PBI matrix. The exfoliated dispersion of 3 and 5 wt% m-MMT in PBI matrix is further proved in Fig. 2a and b, respectively.

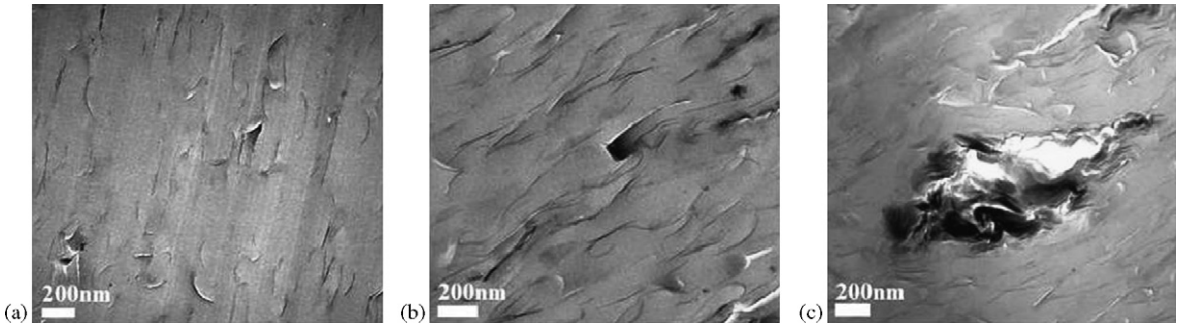

Fig. 2. TEM micrographs of PBI/3 wt% m-MMT nanocomposote (a) PBI/5 wt% m-MMT nanocomposite (b) and PBI/7 wt% m-MMT nanocomposite (c).

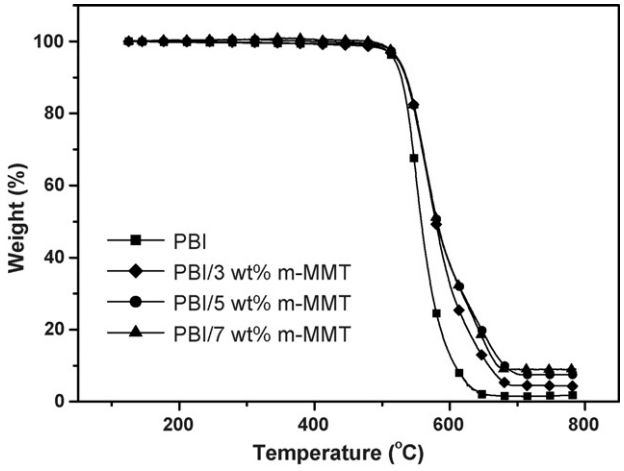

Fig. 3. TGA thermograms of PBI/m-MMT nanocomposite membranes in air.

The estimated size of the silicate layers is ∼1 nm in thickness and 30–400 nm in length. The aggregation of silicate layers is observed in PBI/7 wt% m-MMT nanocomposite in Fig. 2c. The result shows that the content of m-MMT is too much when it is added to 7 wt% in the PBI matrix.

3.3. Thermal properties of PBI/m-MMT nanocomposite membranes

The thermooxidative stability of PBI/m-MMT nanocomposites was studied with TGA in air, as shown in Fig. 3. The pure PBI displayed high thermooxidative stability. The thermooxidative decomposition behavior of PBI/m-MMT nanocomposites was similar to that of pure PBI. The 5% weight loss temperature of PBI, PBI/3 wt% m-MMT, PBI/5 wt% m-MMT and PBI/7 wt% m-MMT were 518, 522, 524 and 523 °C, respectively. The decomposition temperature of PBI/m-MMT nanocomposites shifted to a slightly higher temperature, which indicated that the thermooxidative stability of PBI membranes could be increased slightly with the increase of m-MMT content.

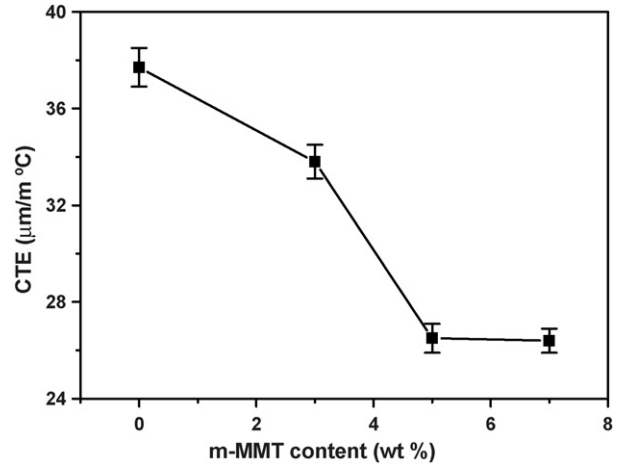

Fig. 4. In-plane coefficients of thermal expansion (CTEs) of the PBI/m-MMT nanocomposite membranes measured in the temperature range of 100–250 °C.

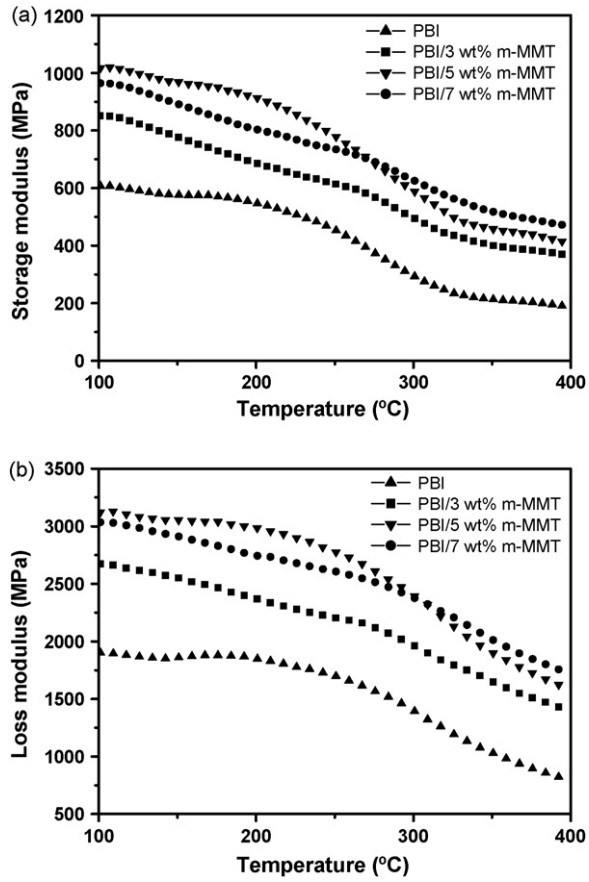

Fig. 5. Storage modulus (a) and loss modulus (b) of PBI/m-MMT nanocomposite membranes.

The in-plane CTEs of PBI/m-MMT nanocomposite membranes are displayed in Fig. 4. The CTE of pristine PBI film was 37.7 ($\mu m\,m^{-1}\,°C$). It was found that the CTEs of PBI/m-MMT nanocomposite films decreased with increasing amounts of m-MMT. The CTE of PBI/7 wt% m-MMT nanocomposite was reduced to 26.4 ($\mu m\,m^{-1}\,°C$), a decrease of 30% relative to that of pure PBI. It indicated that the layered silicates could reduce the thermal expansion of PBI.

The storage modulus and loss modulus of PBI/m-MMT nanocomposite membranes are presented in Fig. 5. The storage modulus and loss modulus of PBI/m-MMT nanocomposite films increased with increasing amounts of m-MMT. They reached maximum values when 5 wt% m-MMT was added in PBI matrix. This implied that there was a strong interaction between the m-MMT and the PBI chains. The $\tan\delta$ of PBI/m-MMT nanocomposite membranes is shown in Fig. 6. The $\tan\delta_{max}$ was identified as the glass transition temperature (T_g). The T_g of pure PBI was 326 °C, which could not be found in the differential scanning calorimeter (DSC) measurement. The T_g of PBI/m-MMT nanocomposite membranes did not increase with the increase of m-MMT content. That could be due to the inherent rigidity of the PBI molecular chains, so the added m-MMT cannot alter it to any further extent.

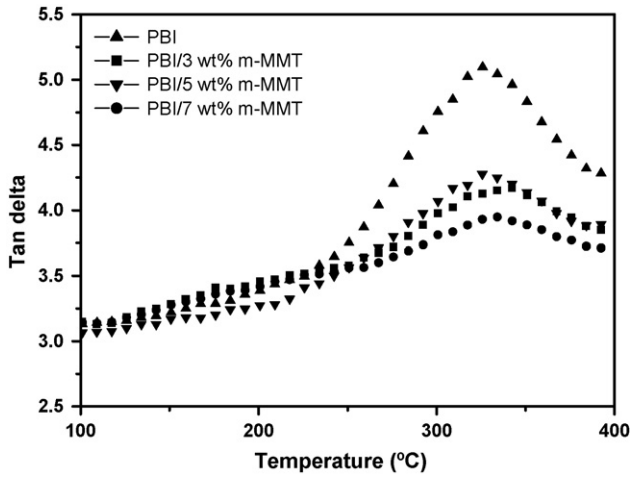

Fig. 6. tan δ of PBI/m-MMT nanocomposite membranes.

3.4. Mechanical properties of PBI/m-MMT nanocomposite membranes

Table 1 summarizes the tensile properties of PBI/m-MMT nanocomposite membranes. The pure PBI film had a tensile modulus of 1.19 GPa, a tensile strength of 55.0 MPa, and a elongation at break of 11.9%. The tensile moduli of PBI/m-MMT films increased with the increase of m-MMT content. The tensile modulus of PBI/5 wt% m-MMT nanocomposite had a 41% increase compared to pure PBI films. This indicated that an exfoliated dispersion of m-MMT could remarkably improve the mechanical properties of PBI membranes. When m-MMT reached 7 wt% in PBI matrix, the tensile modulus of the nanocomposite film had a slight decrease compared to the PBI/5 wt% m-MMT nanocomposite film. The phenomenon might be caused by the aggregation of silicate layers in the nanocomposite film. The tensile strength of the PBI/m-MMT nanocomposite membranes showed a similar trend as their tensile moduli. These results were in good agreement with WAXD and TEM analyses. However, the PBI/m-MMT nanocomposite films were more brittle than the pure PBI films, because of the introduction of ceramic m-MMT. This resulted in the reduction of the elongation at break of PBI/m-MMT nanocomposite films.

Table 1
Mechanical properties of the PBI/m-MMT nanocomposite membranes and phosphoric acid-doped PBI/m-MMT nanocomposite membranes

	Modulus (GPa)	Stress (MPa)	Elongation (%)
PBI	1.19 ± 0.08	55.0 ± 4.7	11.9 ± 1.9
PBI/3 wt% m-MMT	1.54 ± 0.01	66.8 ± 3.3	8.0 ± 1.5
PBI/5 wt% m-MMT	1.68 ± 0.03	70.4 ± 4.7	7.9 ± 0.6
PBI/7 wt% m-MMT	1.55 ± 0.06	66.5 ± 5.7	7.8 ± 1.2
PBI -3.0H_3PO_4	0.31 ± 0.02	23.0 ± 1.5	18.0 ± 1.4
PBI/3 wt% m-MMT -3.0H_3PO_4	0.81 ± 0.01	46.2 ± 3.8	13.8 ± 0.2
PBI/5 wt% m-MMT -3.0H_3PO_4	0.98 ± 0.07	47.3 ± 3.8	11.2 ± 1.8
PBI/7 wt% m-MMT -3.0H_3PO_4	0.77 ± 0.05	32.4 ± 2.1	11.4 ± 2.2

Table 1 also displays the tensile properties of PBI/m-MMT nanocomposite membranes doped with phosphoric acid. Compared to the PBI/m-MMT nanocomposite membranes without phosphoric acid, it was found that the tensile modulus and strength of the films decreased when they were doped with phosphoric acid. This could be due to the plasticizing effect from the phosphoric acid. The tensile modulus of PBI-3.0H_3PO_4 had a 74% decrease relative to the pure PBI films. However, the tensile modulus of PBI/5 wt% m-MMT-3.0H_3PO_4 only decreased by 42% with respect to the PBI/5 wt% m-MMT without doped acid. The tensile strength of PBI/m-MMT nanocomposite membranes doped with phosphoric acid had a similar trend as their tensile moduli. It implied that m-MMT in the PBI matrix could efficiently restrict the plasticizing effect of the phosphoric acid to increase the mechanical properties of the doped PBI membranes.

3.5. Methanol permeability of PBI/m-MMT nanocomposite membranes

Fig. 7 shows the methanol permeability of the PBI/m-MMT nanocomposite membranes. The methanol permeability of the pure PBI membrane was 3.28×10^{-8} ($cm^2\,s^{-1}$). The methanol permeability of the PBI/m-MMT nanocomposite films decreased obviously with increasing amounts of m-MMT. At a 5 wt% loading of m-MMT, the permeability of the nanocomposite films was reduced to 6.2×10^{-9} ($cm^2\,s^{-1}$). It was decreased by approximately 81% with respect to the pure PBI membranes. This indicated that an exfoliated dispersion of m-MMT could remarkably improve the methanol barrier ability of PBI due to a winding diffusion pathway for methanol. When the loaded amount of m-MMT was more than 7 wt% in the PBI matrix, the permeability increased when compared to the PBI/5 wt% m-MMT nanocomposite

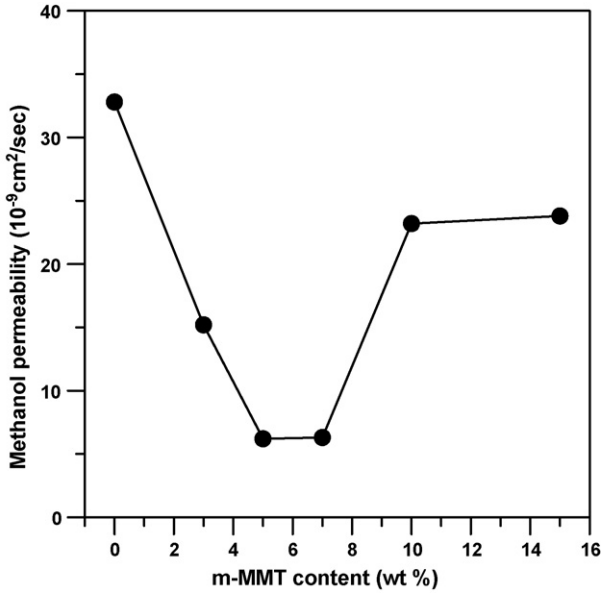

Fig. 7. Methanol permeability of PBI/m-MMT nanocomposite membranes in 6 wt% methanol aqueous solution at room temperature.

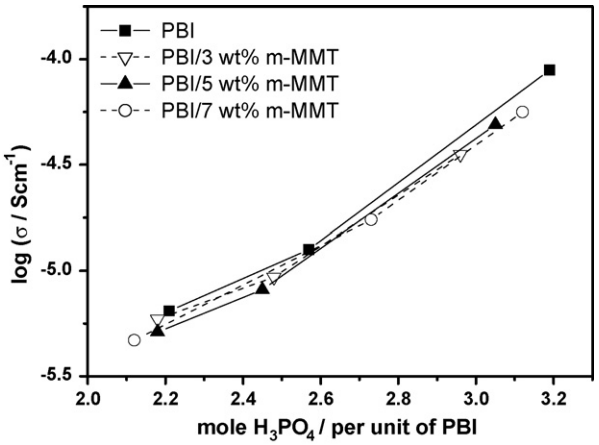

Fig. 8. Proton conductivity (σ) of PBI/m-MMT nanocomposite membranes doped with different amounts of phosphoric acid at 160 °C under anhydrous condition.

film. This result implied that the aggregation of the silicate layers in the nanocomposite film could not effectively decrease the methanol permeation relative to their exfoliated dispersion.

3.6. Conductivity of PBI/m-MMT nanocomposite membranes

Fig. 8 shows the proton conductivity of PBI/m-MMT nanocomposite membranes doped with different amounts of phosphoric acid. The measurement was taken at 160 °C under anhydrous condition, because the proton conductivity of the PBI films doped with phosphoric acid could achieve maximum at that temperature as shown in our previous research [29]. The conductivity of the acid-doped PBI/m-MMT nanocomposite membranes increased with the doping level of phosphoric acid. However, the conductivity of the nanocomposite films was slightly lower than the acid-doped pure PBI, because the m-MMT dispersed in polymer matrix might retard the mobility of protons in the membranes. It was decreased by 21–27% with respect to the acid-doped pure PBI.

4. Conclusions

PBI/MMT nanocomposite membranes can be prepared from a fluorine-containing PBI with organically modified MMT (m-MMT) clay due to the solubility of the fluorine-containing PBI. The addition of m-MMT can significantly enhance the mechanical properties of the phosphoric acid-doped PBI membranes, and reduce the methanol permeability. Although the conductivity is slightly decreased by the m-MMT, the reduction of conductivity by the m-MMT is relatively small compared to the decrease of methanol permeability and the increase of mechanical properties. Therefore, the overall performance of the nanocomposite membranes is still obviously improved by the addition of m-MMT. The PBI/m-MMT nanocomposite membranes have the potential for use as the proton exchange membranes in DMFC.

Acknowledgements

The financial support provided by the National Science Council (Taiwan, ROC) through project NSC95-2216-E-006-341 is greatly appreciated.

References

[1] G. Inzelt, M. Pineri, J.W. Schultze, M.A. Vorotyntsev, Electrochim. Acta. 45 (2000) 2403.
[2] M. Rikukawa, K. Sanui, Prog. Polym. Sci. 25 (2000) 1463.
[3] L. Jorisen, V. Gogel, J. Kerres, J. Garche, J. Power Sources 105 (2002) 267.
[4] D.H. Jung, S.Y. Cho, D.H. Peck, D.R. Shin, J.S. Kim, J. Power Sources 118 (2003) 205.
[5] J.T. Wang, J.S. Wainright, R.F. Savinell, M. Litt, J. Appl. Electrochem. 26 (1996) 751.
[6] P. Staiti, M. Minutoli, J. Power Sources 94 (2001) 9.
[7] J.S. Wainright, J.T. Wang, D. Weng, R.F. Savinell, M. Litt, J. Electrochem. Soc. 142 (1995) L121.
[8] D.J. Jones, J. Roziere, J. Membr. Sci. 185 (2001) 41.
[9] J.A. Asensio, S. Borros, P. Gomez-Romero, J. Polym. Sci. Part A Polym. Chem. 40 (2002) 3703.
[10] L. Xiao, H. Zhang, T. Jana, E. Scanlon, R. Chen, E.W. Choe, L.S. Ramanathan, S. Yu, B.C. Benicewicz, Fuel Cells 5 (2005) 287.
[11] H.J. Kim, S.J. An, J.Y. Kim, J.K. Moon, S.Y. Cho, Y.C. Eun, H.K. Yoon, Y. Park, H.J. Kweon, E.M. Shin, Macromol. Rapid Commun. 25 (2004) 1410.
[12] A. Schechter, R.F. Savinell, Solid State Ionics 147 (2002) 181.
[13] M. Kawahara, J. Morita, M. Rikukawa, K. Sanui, N. Ogata, Electrochim. Acta 45 (2000) 1395.
[14] J.M. Bae, I. Honma, M. Murata, T. Yamamoto, M. Rikukawa, N. Ogata, Solid State Ionics 147 (2002) 189.
[15] J.H. Chang, J.H. Park, G.G. Park, C.S. Kim, O.O. Park, J. Power Sources 124 (2003) 18.
[16] G.W. Zhang, Z.T. Zhou, J. Membr. Sci. 261 (2005) 107.
[17] J.M. Thomassin, C. Pagnoulle, G. Caldarella, A. Germain, R. Jerome, J. Membr. Sci. 270 (2006) 50.
[18] M.K. Song, S.B. Park, Y.T. Kim, K.H. Kim, S.K. Min, H.W. Rhee, Electrochim. Acta 50 (2004) 639.
[19] R.F. Silva, S. Passerini, A. Pozio, Electrochim. Acta 50 (2005) 2639.
[20] C.H. Rhee, H.K. Kim, H. Chang, J.S. Lee, Chem. Mater. 17 (2005) 1691.
[21] D.W. Kim, H.S. Choi, C.J. Lee, A. Blumstein, Y.K. Kang, Electrochim. Acta 50 (2004) 659.
[22] A. Gu, S.W. Kuo, F.C. Chang, J. Appl. Polym. Sci. 79 (2001) 1902.
[23] A. Sasaki, J.L. White, J. Appl. Polym. Sci. 91 (2004) 1951.
[24] R.H. Vora, P.K. Pallathadka, S.H. Goh, T.S. Chung, Y.X. Lim, T.K. Bang, Macromol. Mater. Eng. 288 (2003) 337.
[25] M.O. Abdalla, D. Dean, S. Campbell, Polymer 43 (2002) 5887.
[26] D. Homminga, B. Goderis, I. Dolbnya, H. Reynaers, G. Groeninckx, Polymer 46 (2005) 11359.
[27] K. Yano, A. Usuki, A. Okada, T. Kurauchi, O. Kamigaito, J. Polym. Sci. Part A Polym. Chem. 31 (1993) 2493.
[28] H.L. Tyan, Y.C. Liu, K.H. Wei, Chem. Mater. 11 (1999) 1942.
[29] S.W. Chuang, S.L.C. Hsu, J. Polym. Sci. Part A Polym. Chem. 44 (2006) 4508.
[30] S.L.C. Hsu, K.C. Chang, Polymer 43 (2002) 4097.
[31] V. Tricoli, J. Electrochem. Soc. 145 (1998) 3798.
[32] H.Y. Chang, C.W. Lin, J. Membr. Sci. 218 (2003) 295.